IEEE Access
Multidisciplinary ⋮ Rapid Review ⋮ Open Access Journal

Received March 12, 2021, accepted March 19, 2021, date of publication March 24, 2021, date of current version April 5, 2021.

Digital Object Identifier 10.1109/ACCESS.2021.3068425

Drive-Tolerant Current Residual Variance (DTCRV) for Fault Detection of a Permanent Magnet Synchronous Motor Under Operational Speed and Load Torque Conditions

CHAN HEE PARK[1], JUNMIN LEE[1], HYEONGMIN KIM[1], CHAEHYUN SUH[1], MYEONGBAEK YOUN[1], YONGJIN SHIN[1], SUNG-HOON AHN[1,2], AND BYENG D. YOUN[1,2,3]

[1]Department of Mechanical and Aerospace Engineering, Seoul National University, Seoul 08826, Republic of Korea
[2]Institute of Advanced Machines and Design, Seoul National University, Seoul 08826, Republic of Korea
[3]OnePredict Inc., Seoul 06160, Republic of Korea

Corresponding author: Byeng D. Youn (bdyoun@snu.ac.kr)

This work was supported in part by the Basic Research Laboratory Program through the National Research Foundation of Korea (NRF) by the Ministry of Science and ICT (MSIT) under Grant 2021R1A4A2001824, and in part by the Korea Institute for Advancement of Technology (KIAT) by the Ministry of Trade, Industry and Energy (MOTIE) through HRD Program for Industrial Innovation under Grant P0008691.

ABSTRACT This paper proposes a novel method that uses stator current signals to detect motor faults under operational speed and load torque conditions. Previous studies on motor current signature analysis (MCSA) have been devoted to developing methods to detect faults in non-stationary conditions; however, they have limitations. Conventional methods require much domain knowledge or parameter selection for signal decomposition, and are applicable under limited variable conditions. Thus, this paper proposes a new feature, drive-tolerant current residual variance (DTCRV), for fault detection. This new approach requires no domain knowledge and is applicable under varying speed and load torque conditions. In the proposed method, first, the envelope of the current signal is calculated to extract its modulation. Second, the drive-related signal, which greatly varies based on speed and load torque conditions, is extracted from the enveloped current signal. Third, the drive-tolerant current residual (DTCR) is calculated; the DTCR is defined as the subtraction of the drive-related signal from the enveloped current signal. Finally, the new health feature is calculated as the variance of the DTCR. To demonstrate the proposed method, experimental studies were conducted under several operating conditions (i.e., different speed profiles and load torque levels) with two fault modes: 1) a stator inter-turn short and 2) misalignment. Results confirm the ability of DTCRV to promptly and accurately detect faults in a variety of conditions; in contrast, conventional methods are greatly affected by the operating conditions.

INDEX TERMS Current analysis, fault detection, permanent magnet motors, time-varying condition, variable speed.

I. INTRODUCTION

Industrial motors are widely used in lots of manufacturing processes and permanent magnet synchronous motors (PMSMs), which are one type of industrial motors, are usually integrated into many types industrial equipment that perform precise control, such as industrial robots, cooperative robots, and CNC machines [1]–[3]. Since a trivial fault in any of the numerous PMSMs in a manufacturing line can cause huge economic loss due to downtime and defective items, many studies have been conducted to develop a robust fault-detection method for PMSMs [4], [5]. Many studies on fault detection can be categorized as model-based approach and signal processing-based approach in general [6]–[10]. Among several signals that have been used for the signal processing-based fault detection, the stator current signal has emerged as the most generally analyzed signal for monitoring the health condition of PMSMs and

The associate editor coordinating the review of this manuscript and approving it for publication was Shihong Ding.

the load components in rotating systems; this analysis is called motor current signature analysis (MCSA) [11], [12]. Despite continuous development of MCSA, practical application of the approach is difficult in modern industrial systems, where non-stationary operating conditions (i.e., various speeds and load torques) are prevalent [13]–[17]. The signal deformation that results from these variable drive-related conditions makes it difficult to identify the fault-related fluctuations because the drive-related current signals are dominant in the non-stationary conditions of normal operation.

To address this issue, several previous studies have tried to detect motor faults by examining transient current signals. Time-frequency analysis (TFA) represents signals in the time-frequency domain; therefore, the spectral properties of signals can be shown in time-series. Most previous research using TFA has investigated the trend of coefficients according to the particular fault frequency [18]. In [19]–[22], the energy around fault characteristic frequency was computed in Wigner-Ville distribution (WD), and its behavior on speed and load variations were investigated. Similarly, the harmonic order tracking method was developed to identify rotor faults using Garbor transformed current signals [23]. The TFA-based approaches, however, require motor-specific domain knowledge (e.g., fault frequencies, the number of poles, rotating frequencies) and usually time-consuming. The signal decomposition-based approaches can be one of the ways to avoid the challenge of TFA-based approaches. The discrete wavelet transform (DWT), which decomposes a signal using high- and low-pass filters with particular mother wavelets, was applied to detect a motor fault by utilizing the detail signals in DWT that revealed the fault patterns [24]–[27]. In [28], DWT decomposed the current signal of which the fundamental component was removed by the adaptive filter to detect faults under variable driving conditions. Also, the intrinsic mode function (IMF) calculated by empirical mode decomposition (EMD) was investigated to extract the information related to faults in the current signals. Several fault indicators were developed to detect faults under non-stationary condition, such as the degree of fluctuations of IMFs [29], [30], the energy of IMFs [31], and the instantaneous amplitude of IMFs computed by the Hilbert-Huang transform (HHT) [32], [33]. The signal decomposition-based approaches, however, demand the selection of the particular bandwidth or decomposition level that is sensitive to the fault. Furthermore, the aforementioned TFA-based and signal decomposition-based approaches have not been validated to detect faults with one criterion under various speed profiles and various load torque levels simultaneously. Considering that industrial machines operate in various load and speed conditions, the development of robust fault detection methods that can be applied in non-stationary conditions with minimal expertise is still required.

Therefore, this paper proposes a novel method to detect motor faults under variable speed and load torque conditions. In the proposed approach, a drive-tolerant current residual (DTCR), which is defined as the subtraction of the drive-related signal from the enveloped current signal, is used to reflect the health state of a rotating system in a way that is robust to variable driving conditions. First, the Hilbert transform (HT) is used to obtain the envelope of a stator current signal. Next, to extract the drive-related signal, the gradient of the envelope current signal and linear regression are used. Then, a new feature is defined – drive-tolerant current residual variance (DTCRV) – by calculating the variance of the DTCR. The work outlined in this paper offers four primary contributions:

1) The proposed DTCRV feature can detect faults under operational speed profiles and various load torque conditions. This is meaningful because most real-world data are acquired under unconstrained driving conditions.
2) The proposed DTCRV method is practical in that both the motor-specific domain knowledge and the parameter selection for signal decomposition are not required.
3) The proposed DTCRV method can be applied with less computational cost, as compared to the TFA-based approach.
4) The proposed DTCRV method is demonstrated through experiments that study both mechanical and electrical faults under several driving conditions using PMSMs.

The remainder of this paper is organized as follows. Section II summarizes the background required to understand the proposed method. The proposed method is described in detail in Section III. In Section IV, the effectiveness of the proposed method is confirmed through two experimental studies: 1) a stator inter-turn short and 2) misalignment. Section V summarizes the conclusions of the paper.

II. BACKGROUNDS

This section briefly explains the background of the stator current signal from the perspective of operating conditions and for fault diagnosis. Next, several previous studies that have used the stator current signals for fault diagnosis are summarized; further, we outline the challenges of the prior methods when applied in various speed and load torque conditions.

A. THE RELATION OF THE STATOR CURRENT AND DRIVING CONDITIONS

The electromagnetic torque T_e is a torque produced by the interaction between the magnetic field and the stator current in a motor. For a PMSM, T_e can be expressed as [34]

$$T_e = \frac{3p}{2}[\phi i_q + (L_d - L_q) i_d i_q] \tag{1}$$

where p is the number of poles, ϕ is the flux linkage generated by the permanent-magnet poles of the rotor, i_d, i_q and L_d, L_q are the stator currents and inductances of the d- and q-axis, respectively. i_d and i_q are the values converted from the three-phase stator currents using dq-transform for pursuing convenience in control. In the case of field-oriented control systems, which are generally used for servo-systems, i_q is

TABLE 1. Fault characteristic features in the current spectrum.

Fault mode	Fault characteristic frequencies in the current spectrum f_c
Stator inter-turn short	f_c=3f_s [16], [38], [39], $f_s \pm nf_r$ [40], [41]
Mechanical faults caused by load torque oscillation (e.g., unbalance, misalignment, bearing faults)	f_c=$f_s \pm nf_r$ [19]–[23]

interpreted to be proportional to T_e, because the flux of the d-axis is controlled to be continuously aligned with i_d [35]. Considering the surface-mounted PMSM, which has the same L_d and L_q value, T_e and the electromechanical torque equation can be expressed as

$$T_e(t) = ki_q(t) = J\frac{d}{dt}\omega_r(t) + B\omega_r(t) + T_L(t) \quad (2)$$

where k is the torque constant, J is the inertia of the rotating system, B is the friction coefficient, $\omega_r(t)$ is the rotating speed, and $T_L(t)$is the load torque. From (2), the driving conditions (i.e., load component, velocity, and acceleration) are confirmed to affect not only $T_e(t)$, but also $i_q(t)$, which is the converted value of the stator current signals.

B. STATOR CURRENT SIGNATURE DUE TO FAULTS

Several mechanical faults, (e.g., misalignment, unbalance and bearing wear) make the airgap non-uniform [20]. This state is called eccentricity. The non-uniform airgap affects the permeance, which is inversely related to the airgap length as

$$\Lambda(t,\theta) = \frac{\mu_0}{g}(1 + \delta_s\cos(\theta - \varphi_s) + \delta_d\cos(\omega_r t - \theta)) \quad (3)$$

where, μ_0 is the permeability of air, g is the nominal airgap length, φ_s is the angle of the minimum airgap position due to the static eccentricity, and θ is the circumference angle. δ_s and δ_d are the normalized degree of static and dynamic eccentricity [36], [37]. Considering the fundamental harmonic term, the magnetomotive force (MMF) can be approximated as

$$F(t,\theta) = F_1(t)\cos(\omega t - p\theta) \quad (4)$$

where $F_1(t)$ denotes the major amplitude of MMF, and ω is the electric rotating speed. Then, the airgap flux density B is defined as the product of MMF and the permeance as

$$\begin{aligned} B(t,\theta) &= F(t,\theta)\cdot\Lambda(t,\theta) \\ &= K_B(t)[B_c + B_m\cos(\omega_r t - \theta)]\cos(\omega t - p\theta) \quad (5) \\ V(t) &= RI(t) + \frac{d}{dt}\Phi(t) \quad (6) \end{aligned}$$

where $K_B(t)$ is F_1 (t) μ_0/g, B_c is $1+\delta_s\cos(\theta - \varphi_s)$, B_m is δ_d, R is stator resistance, and $V(t)$ is power supply voltage. As B is the derivative of the flux $\Phi(t)$, the stator voltage equation (as in (6)) implies that the major component of the stator current can be expressed as

$$\begin{aligned} I(t) &= K_I(t)[I_c + I_m\cos(\omega_r t - \varphi_m)]\cos(\omega t - \nu) \\ &= I_1(t)\cos(\omega t - \nu) + \alpha I_1(t)\cos((\omega \pm \omega_r)t - \varphi) \quad (7) \end{aligned}$$

where $K_I(t)$, I_c, and I_m are the corresponding terms of $K_B(t)$, B_c, and B_m, respectively. $I_1(t)$, φ, φ_m and ν are the coefficients and phases of the stator current's major components, including the terms related to the static and dynamic eccentricity, and α is the modulation index. Based on (7), the faults can be confirmed by investigating the amplitude modulation (AM) in the stator current signals. Also, the electrical faults represented by stator turn shorts affect the stator current by showing odd multiples of the supply frequency's third harmonics [16], [38], [39], or AM of the rotating frequency [40], [41]. Therefore, the AM of the stator current can be observed in both the mechanical and electrical fault states of a rotating system.

C. BRIEF REVIEW OF FAULT DIAGNOSIS USING THE STATOR CURRENT IN TIME-VARYING CONDITIONS

TABLE 1 summarizes the fault characteristic frequencies f_c in the current spectrum, which were used in previous studies, where f_s, f_r are the supply and rotating frequency, respectively, and n = 1,2,3,... Since f_c cannot be applied to non-stationary conditions directly due to the time-varying f_s and f_r, several studies have conducted TFA to track the magnitude of f_c in the time-frequency domain [19], [22], [23]. In particular, WD has been widely used to calculate the features in the time-frequency domain [19], [22], and pseudo-WVD (PWD) often replaces WD to compensate for interference terms in practical applications [20]. For example, the energy of $3f_s$ could be extracted for investigating stator inter-turn shorts; the energy around $f_s \pm f_r/2$ could be calculated to investigate mechanical faults using PWD. These TFA-based approaches require several motor-specific information and the speed profile to compute the time-varying characteristic frequencies. Therefore, signal decomposition techniques (e.g., DWT [24]–[28], EMD [29]–[31], HHT [32], [33]) have been adopted to readily extract the fault-related components. When DWT was used, the energy of the specific detail signals could be calculated for the health feature [26], [27]. The specific detail signals were selected based on an observation of the fault-pattern. When EMD [29]–[31] or HHT [32], [33] was used, the IMFs that reveal the fault-related components were investigated after decomposing the drive-related components in the preceding IMFs. However, the observation of the appropriate decomposed signals containing fault information is difficult for the signal decomposition based approach. In addition, most of the aforementioned studies were validated under only

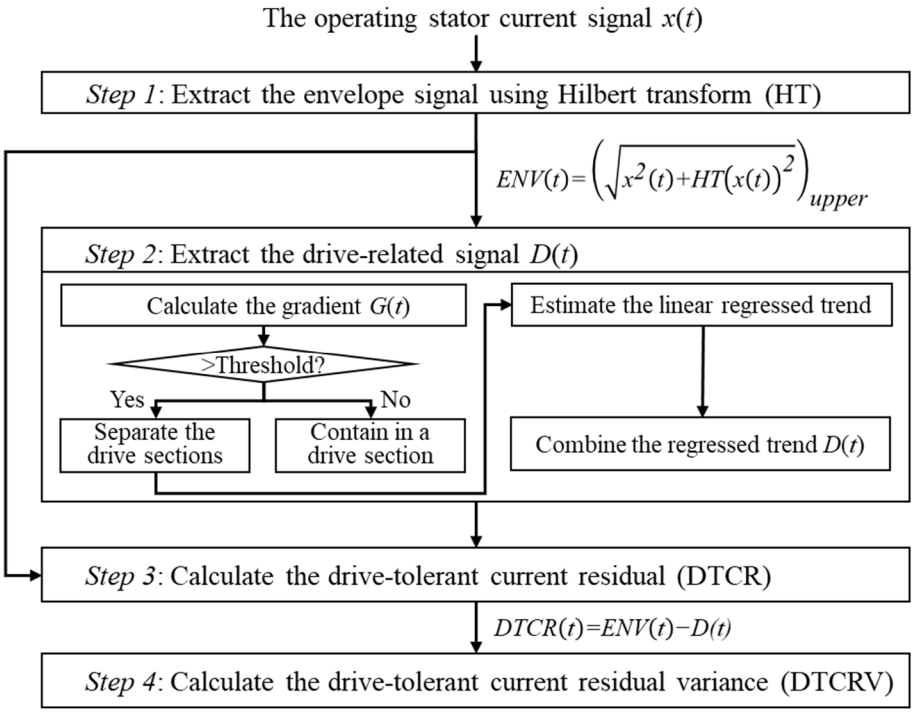

FIGURE 1. A framework of the proposed DTCRV method.

variable-speed profiles. Therefore, the application of these conventional methods for real driving conditions – in which the speed varies under several load torque conditions – is uncertain.

III. THE PROPOSED DTCRV METHOD

This section presents the proposed DTCRV method to detect faults under operational speed and load torque conditions. Fig. 1 offers a flowchart of the proposed method. The details of each step are described in Sections A and B, focusing on the principle of the proposed method. In Section C, the contribution and advantages of the proposed method are explained with the comparison of the conventional methods.

A. EXTRACTION OF THE DRIVE-RELATED SIGNAL

Since the raw stator current signal consists of a fundamental driving sinusoidal wave and other harmonics that can be generated by the controller, faults, or other factors, the envelope of the raw stator current signal is firstly extracted. Based on (7), the major component of the raw stator current signal can be expressed as

$$x(t) = I_1(t)\cos(2\pi f_s t)+\alpha I_1(t)\cos(2\pi(f_s \pm f_k)t+\varphi_k) \quad (8)$$

where α is the modulation index; f_k and φ_k are the frequency and phase angle of the fault, respectively. Then, the analytic signal of $x(t)$ using HT can be related to the amplitude of the enveloped current signal as

$$x_a(t) = x(t) + j\hat{x}(t) = x_m(t)e^{j\psi(t)} \quad (9)$$

where $x_a(t)$is the analytic signal of $x(t)$, $\hat{x}(t)$ is the HT result of $x(t)$ that is $\pi/2$ phase-shifted, $x_m(t)$ is the amplitude of $x_a(t)$, and $\psi(t)$ is the instantaneous phase. Based on Section II-B, the information about the fault-related AM is expected to be carried in $x_m(t)$. $x_m(t)$ conserves the magnitudes of $x(t)$, while it reduces the effect of high-frequency noises that are usually induced from a variable frequency drive. In this study, the upper signal of $x_m(t)$, denoted as $ENV(t)$, is used.

Next, the drive-related signal is extracted from $ENV(t)$. In a balanced three-phase system, the magnitude of $x_m(t)$ is proportional to $T_e(t)$; therefore, $ENV(t)$ can be expressed from (2) as

$$ENV(t) \propto ki_q(t) \quad (10)$$

Based on the fact that $i_q(t)$ is the result of dq-transformation of the three-phase $x(t)$, $i_q(t)$ can be written from (8) as

$$\begin{aligned} i_q(t) &= I_1(t)\cos(2\pi f_s t-\theta_0)+\alpha I_1(t)\cos(2\pi(f_s\pm f_k)t+\varphi_k-\theta_0) \\ &= I_1(t)\cos(\theta_p) + \alpha I_1(t)\cos(\pm 2\pi f_k t+\varphi') \end{aligned} \quad (11)$$

where θ_0 is set to $2\pi f_s t+\theta_p$; θ_p is the constant phase angle, and $\varphi'$is $\varphi_k-\theta_p$. Also, the right-hand side of (2) can be rewritten to include the torque oscillations and spatial harmonics as

$$(J\frac{d}{dt}\omega_r(t)+B\omega_r(t)+T_c) + \sum_{n=1}^{\infty} T_n(t)\cos(2\pi f_n t+\varphi_n) \quad (12)$$

where T_c is the constant load torque, T_n, f_n, and φ_n are the amplitude, frequency, and phase angle for torque

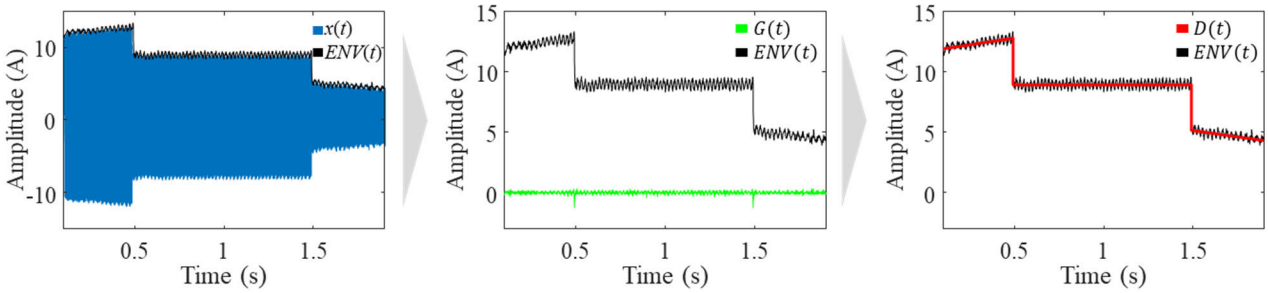

FIGURE 2. The procedure of extracting $D(t)$ from $ENV(t)$.

oscillations respectively. When (11) and (12) are incorporated into (2), the torque-current mechanism can be described as

$$kI_1(t)\cos(\theta_p) + k\alpha I_1(t)\cos(\pm 2\pi f_k t + \varphi') = (J\frac{d}{dt}\omega_r(t) + B\omega_r(t) + \mathrm{T}_c) + \sum_{n=1}^{\infty}\mathrm{T}_n(t)\cos(2\pi f_n t + \varphi_n) \quad (13)$$

Sequentially the first term in the left-hand side corresponds to the first term in the right-hand side, which is related to the driving condition. Also, $ENV(t)$ is proportional to (13) based on (10) as

$$ENV(t) \propto (J\frac{d}{dt}\omega_r(t) + B\omega_r(t) + \mathrm{T}_c) + \sum_{n=1}^{\infty}\mathrm{T}_n(t)\cos(2\pi f_n t + \varphi_n) \quad (14)$$

The first term in the right-hand side of (14) can be matched to the dominant linear trend of $ENV(t)$ in the case of constant acceleration. Although the motion of manufacturing machines is complicated, the speed profile of a servo motor usually consists of constant acceleration, short or no constant speed, and deceleration.

Fig. 2 shows the procedure of extracting the dominant trend from $ENV(t)$ in the driving condition, which consists of constant acceleration, constant speed, and constant deceleration. The dominant trend of $ENV(t)$ changes linearly as the speed changes linearly in a uniform acceleration region. When the driving condition changes from acceleration to stationary, $ENV(t)$ changes rapidly as $Jd\omega_r(t)/dt$ in (14) disappears and becomes proportional to the level of load torque. Based on the association of the dominant trend of $ENV(t)$ and the driving condition, the linear trend of $ENV(t)$ is determined to be the drive-related signal $D(t)$. Before extracting $D(t)$, the gradient of $ENV(t)$, which is denoted as $G(t)$, is computed for subdivision. When the driving condition is switched, $ENV(t)$ changes drastically; thus, the transition time can be captured at the large gradient points. After subdividing $ENV(t)$ into several sections, linear regressions of $ENV(t)$ in each section are calculated. Then, $D(t)$ is defined as the union of linear estimation. In Fig. 2., $G(t)$ has two peak points at the transition time, and $D(t)$ can be determined as the combination of the linear estimations in three subsections that $G(t)$ divides.

Unlike the previous approaches that decomposed the non-stationary current signal empirically or removed the fundamental current signal using specific filters, the proposed DTCRV method readily extracts the drive-related components which are induced from the torque-current mechanism. The linear regressed $D(t)$ is a strict equation-based extraction; however, several filters (e.g., moving average or low-pass) can be substituted for the linear regression and applied to various driving conditions.

B. DRIVE-TOLERANT CURRENT RESIDUAL

Using $D(t)$ which is determined in advance, the drive-tolerant current residual $DTCR(t)$ can be calculated by the subtraction of $D(t)$ from $ENV(t)$ as

$$DTCR(t) = ENV(t) - D(t) \quad (15)$$

After $D(t)$ is subtracted, the dependence of DTCR on the driving condition becomes small; therefore, the influences that are not related to the driving conditions are prominent in the DTCR. Also, the fluctuations caused by faults receive more attention. Then, the variance is calculated to arrive at a representation of DTCR, which is defined as

$$\mathrm{DTCRV} = E(|DTCR(t) - \mu|^2) \quad (16)$$

where μ is the average of $DTCR(t)$. DTCRV can be interpreted as the energy of the DTCR, since the energy of the time-series signal is usually defined as a summation of the squared signal and the mean of the DTCR would be zero in the ideal case. When $D(t)$ does not include all time-varying effects, the DTCR could have a bias induced by a complicated driving condition; thus, the variance can compensate for the bias error of the DTCR.

C. THE CONTRIBUTION AND ADVANTAGES OF DTCRV

Through the proposed DTCRV method, the stator current signals under operational driving conditions can be readily utilized to evaluate the health condition of a motor. It is beneficial that the DTCRV method, which is developed on the basis of physical relations between the torque and current

TABLE 2. Comparison of the proposed DTCRV and two conventional approaches.

	Proposed (DTCRV)	TFA-based approach (e.g. PWD)	Signal decomposition-based approach (e.g. DWT, EMD, HHT)
Required information about the fault	None	Fault characteristic frequency	Decomposition level that fault patterns reveal
Required information about the driving conditions	None	Speed profile Load torque (optional)	Load torque (optional)
Parameter dependency	Low	Low	High
Time-cost	Low	High	Low

of a motor, can be applied with less expertise. To precisely describe the contribution and advantages of the DTCRV, it is compared with two conventional approaches (i.e., TFA-based and signal decomposition-based). TABLE 2 summarizes the comparisons described below. The proposed DTCRV method does not require any information about the fault. In contrast, the two conventional approaches are based on the extraction of fault-related components. Therefore, the two conventional methods are limited to situations where the fault-related information is pre-assigned, such as fault characteristic frequency over time and the decomposition level that the fault patterns reveal. The DTCRV method also does not require any information about the driving condition; instead, it adaptively decreases the effect of speed and load torque conditions by subtracting the linear components in the current envelope. For the TFA-based approach, the speed profile is essential for calculating the characteristic frequency. The load torque condition is optionally used to attempt to compensate for its influence. Furthermore, the DTCRV is less susceptible to the parameter settings and its time-cost is low because the entire process of DTCRV is automatically handled in the time-domain. In contrast, the time-cost for the TFA-based approach is high due to the computation of many convolutions. The signal decomposition-based approach is highly affected by several parameters, such as the type of wavelet function and the appropriate band using the DWT method, or the selection of proper IMFs using the EMD and HHT methods. Finally, the DTCRV method can highlight the current fluctuations through the automatic reduction of drive-related signals.

IV. EXPERIMENTAL STUDIES

To validate the effectiveness of the proposed method, two experimental studies were explored: 1) a stator inter-turn short (SIS) and 2) misalignment (MSGN). This section first describes the experimental settings used to acquire the datasets and then discusses the results of the proposed method. Both cases also include a comparative analysis with other previously published health features, which were described in Section II-C, to confirm the superiority of the proposed method.

A. DESCRIPTION OF THE EXPERIMENTAL SETUP

For the target motor, a 200W-5.5Nm, 20-pole, surface-mounted PMSM embedded in 4th axis of a cooperative robot was used (See Fig. 3 (a), (c)). Fig. 3(b) shows the test rig setup used in the experiment. The target PMSM was position-controlled using an incremental encoder, of which the resolution was 4000 pulses per revolution. A hysteresis brake (Magtrol, BHB-3BA) was connected to the motor shaft via couplings; a torque meter (Unipulse, UTM-II) was installed between two couplings to measure torque and speed. The three-phase stator current signals were measured by current probes (Tektroniks, A622), which were mounted between the servo drive and the motor. All signals were collected with a sampling rate of 12.8 kSa/s using an NI-system (C-RIO9066). All driving conditions that were used in the experiment are summarized in TABLE 3; two speed profiles (named trapezoidal and triangle) with five load torque conditions (0%, 30%, 50%, 70%, 100% of the rated load torque),

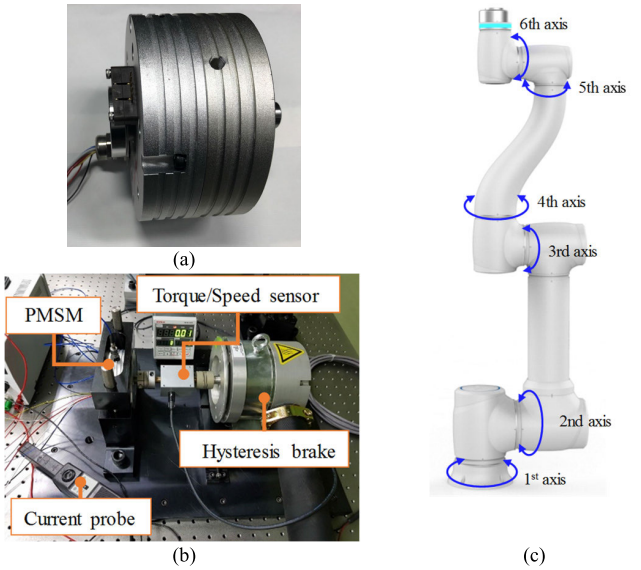

FIGURE 3. Experimental setup: (a) target PMSM, (b) the configuration of the test-bed, (c) the robot in which the target PMSM is embedded (4th axis).

TABLE 3. The experimental conditions.

State	Fault level	Speed profile	Load torque (%)				
NOR	0	Trapezoidal Triangle	0	30	50	70	100
SIS1	1	Trapezoidal Triangle	0	30	50	70	100
SIS2	2	Trapezoidal Triangle	0	30	50	70	100
MSGN1	1	Trapezoidal Triangle	0	30	50	70	100
MSGN2	2	Trapezoidal Triangle	0	30	50	70	100

respectively, were studied. The trapezoidal profile was configured by controlling a motor with 100 revolutions in 3 seconds, and the triangle profile was configured by controlling a motor with 50 revolutions in 2 seconds. Among all experimental conditions, the three load torque conditions (0%, 50%, 100%) of each speed profile in normal (NOR) and fault level 2 are described in the figures for representative comparison.

B. EXPERIMENT 1: STATOR INTER-TURN SHORT (SIS)

First, an SIS was emulated by coiling the uncovered windings in the production stage. Fig. 4 shows a faulty stator, in which a portion of the windings were chemically uncovered. Two motors with different fault levels, where the degrees of uncovered windings were different, were used in the experiment. TABLE 4 describes the measured impedance (resistance, inductance) of the two SIS and NOR motors; the uncovered windings were coiled up only in the a-phase.

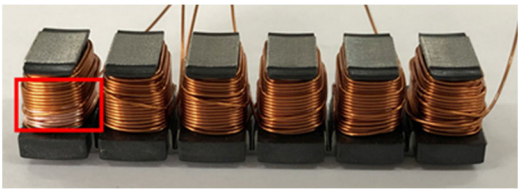

FIGURE 4. Inter-turn short windings of SIS2.

Fig. 5 shows the procedure for calculating DTCR from the raw current signal in several driving conditions of NOR; Fig. 6 shows calculation for SIS2. Comparing the raw current of Fig. 5 and 6, the modulation caused by SIS can be confirmed; the enlarged parts of Fig. 5(b) and Fig. 6(b) obviously show the severity of modulation due to SIS at the constant speed region. From all $ENV(t)$ of each driving condition in Fig. 5 and Fig. 6, it can be seen that $ENV(t)$ was highly influenced by the speed variation and load torque level. The amplitude trend of $ENV(t)$ was largely dominated by the speed variation and was simultaneously proportional to the load torque level. So DTCRs were obtained according to the procedure as described in Fig. 1. $G(t)$, which was calculated to set the criteria for subdividing $ENV(t)$, had peak points when the speed profile was drastically changed, regardless of the health state of the motor. There appeared two peak points in Fig. 5(a-c) and Fig. 6(a-c), while only one appeared in Fig. 5(d-f) and Fig. 6(d-f). Next, $D(t)$ was regressed in each section that the peaks of $G(t)$ divide. Then DTCRs were obtained by subtracting $D(t)$ from $ENV(t)$. The small difference of DTCRs under variable speed and load torque levels indicated the tolerance of DTCR to driving conditions, as shown in DTCRs in Fig. 5. While the difference of DTCRs depending on driving conditions was small in Fig. 6, DTCRs of Fig. 6 highly fluctuated compared to those of Fig. 5. Therefore, we can confirm that the influence of SIS on DTCR was larger than that of the driving conditions. Furthermore, DTCRs were occasionally amplified at the transient regions in the case of SIS. Not only the instantaneous irregularities that occur right after the speed transition but the deterioration of the stator windings where the current flows could aggravate the fluctuation of DTCR, as shown in the transient sections of DTCRs in Fig. 6.

Fig. 7 shows the results of each feature (i.e. E_{PWD}, E_{DWT}, E_{HHT}, and DTCRV), as determined using the PWD, DWT, HHT, and the proposed DTCRV methods, respectively. Each feature was normalized with an average feature value of NOR. E_{PWD}, E_{DWT}, E_{HHT} were calculated based on the conventional methods described in Section II-C. For E_{PWD}, the magnitudes of the coefficients of PWD around *3fs* were mean-squared over time. For E_{DWT}, the fifth detail signal, *d5* was selected and calculated as the sum of squares based on the fact that the frequency band of *d5* was from 1 kHz to 2 kHz, which contains the characteristic frequency in the constant-speed region, of which the fundamental frequency was 500 Hz. For E_{HHT}, the third IMF of the raw current signal was extracted, and the variance of its instantaneous amplitude was computed. As can be seen in Fig. 7, DTCRV outperformed the other methods by detecting SIS with one criterion. E_{PWD} and E_{DWT} had the similar values between two speed profiles, but highly dependent on the load torque

TABLE 4. The impedance of the motors used in the SIS experiment.

Phase			Nor		SIS1		SIS2	
Resistance (Ω)		a	0.37		0.36		0.35	
		b	0.37		0.37		0.38	
		c	0.37		0.37		0.38	
			L	Q	L	Q	L	Q
Inductance (mH)	250 Hz	a	0.33	1.42	0.31	1.30	0.26	1.09
		b	0.33	1.39	0.34	1.42	0.32	1.36
		c	0.32	1.35	0.32	1.37	0.31	1.31
	500 Hz	a	0.33	2.81	0.31	2.36	0.25	1.61
		b	0.33	2.74	0.34	2.79	0.32	2.67
		c	0.32	2.64	0.32	2.68	0.31	2.58

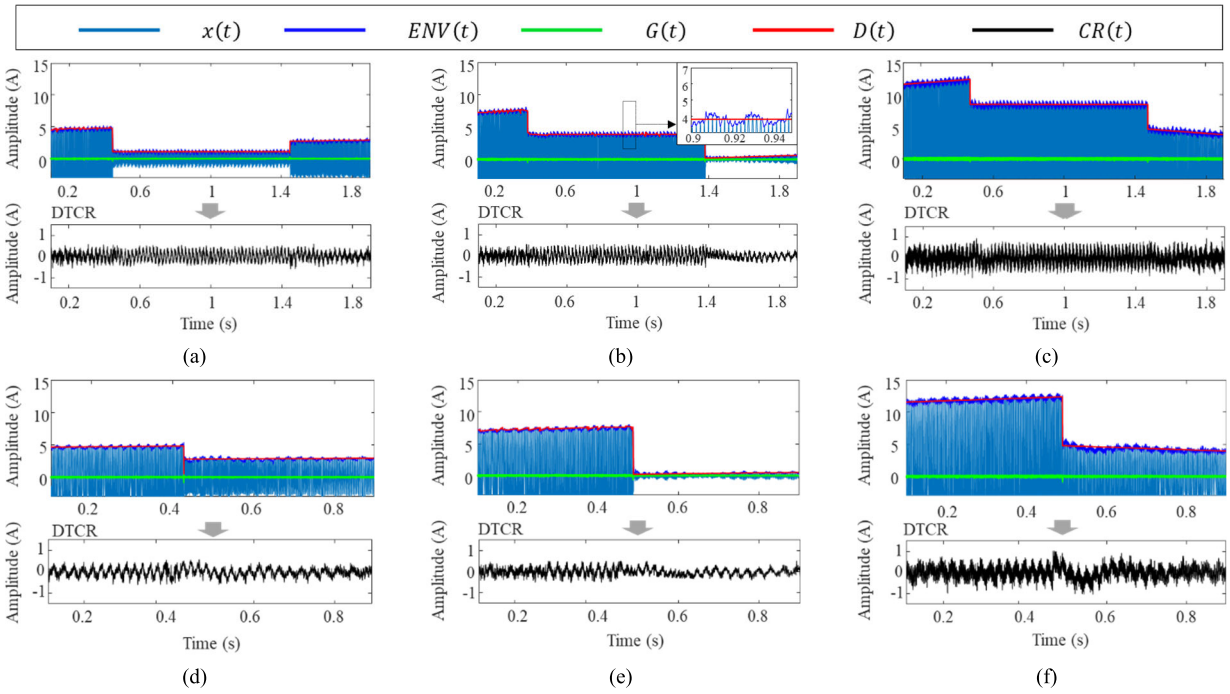

FIGURE 5. The procedure for calculating DTCR in NOR: [speed profile, load torque] (a) [Trapezoidal, 0%], (b) [Trapezoidal, 50%], (c) [Trapezoidal, 100%], (d) [Triangle, 0%], (e) [Triangle, 50%], and (f) [Triangle, 100%].

TABLE 5. Performance of SIS detection and average time-cost for calculating one feature.

	Features	DTCRV (Proposed)	E_{PWD} [19]	E_{DWT} [26]	E_{HHT} [32]
Performance measure	FDR	4.919	0.034	0.027	0.002
	PoS	0.959	0.091	0.082	0.019
Time-cost		0.007±0.002 sec	46.664±4.317 sec	0.004±0.004 sec	0.028±0.005 sec

level as shown in Fig. 7(b, c). Since E_{PWD} and E_{DWT} of SIS in low load torque condition were smaller than those of NOR in high load torque condition, only SIS2 under 100% load torque level was detectable. Through the result, we can determine that the effect of load torque condition was difficult to be suppressed or separated using PWD or DWT. E_{HHT} showed the deficient performance with widespread values in all driving conditions (See Fig. 7(d)). The inferior performance of E_{HHT} might be due to the unstable extraction of IMF which is conducted empirically.

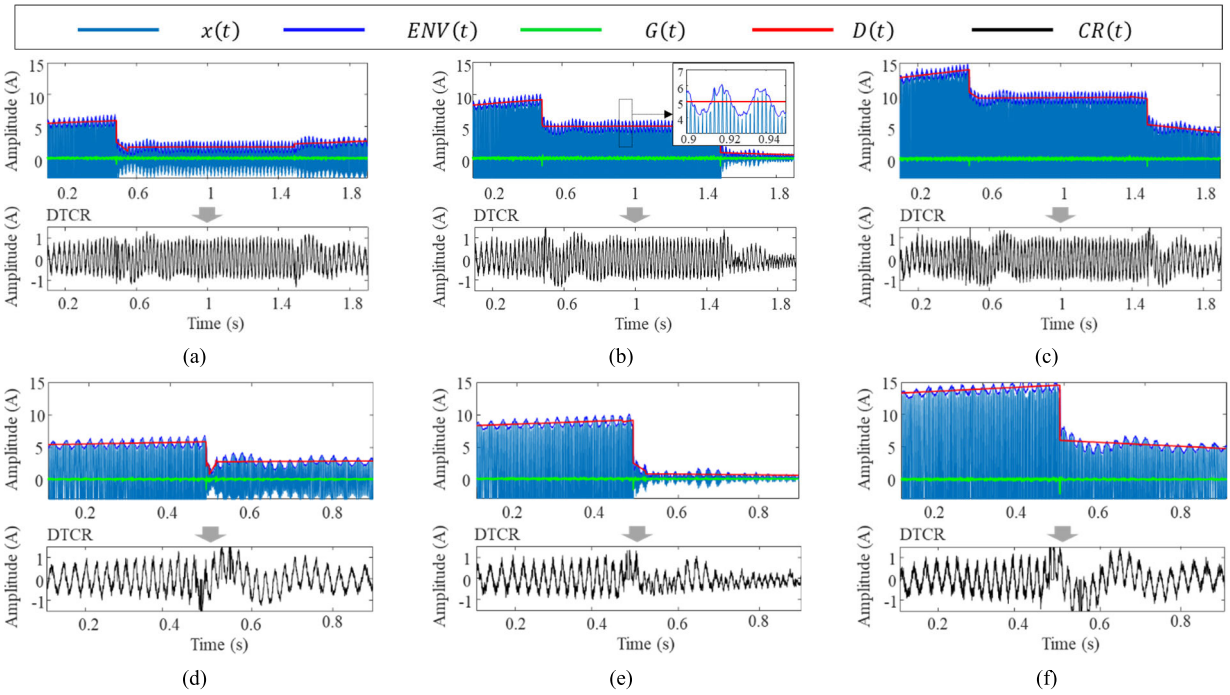

FIGURE 6. The procedure for calculating DTCR in SIS2: [profile, load torque] (a) [Trapezoidal, 0%], (b) [Trapezoidal, 50%], (c) [Trapezoidal, 100%], (d) [Triangle, 0%], (e) [Triangle, 50%], and (f) [Triangle, 100%].

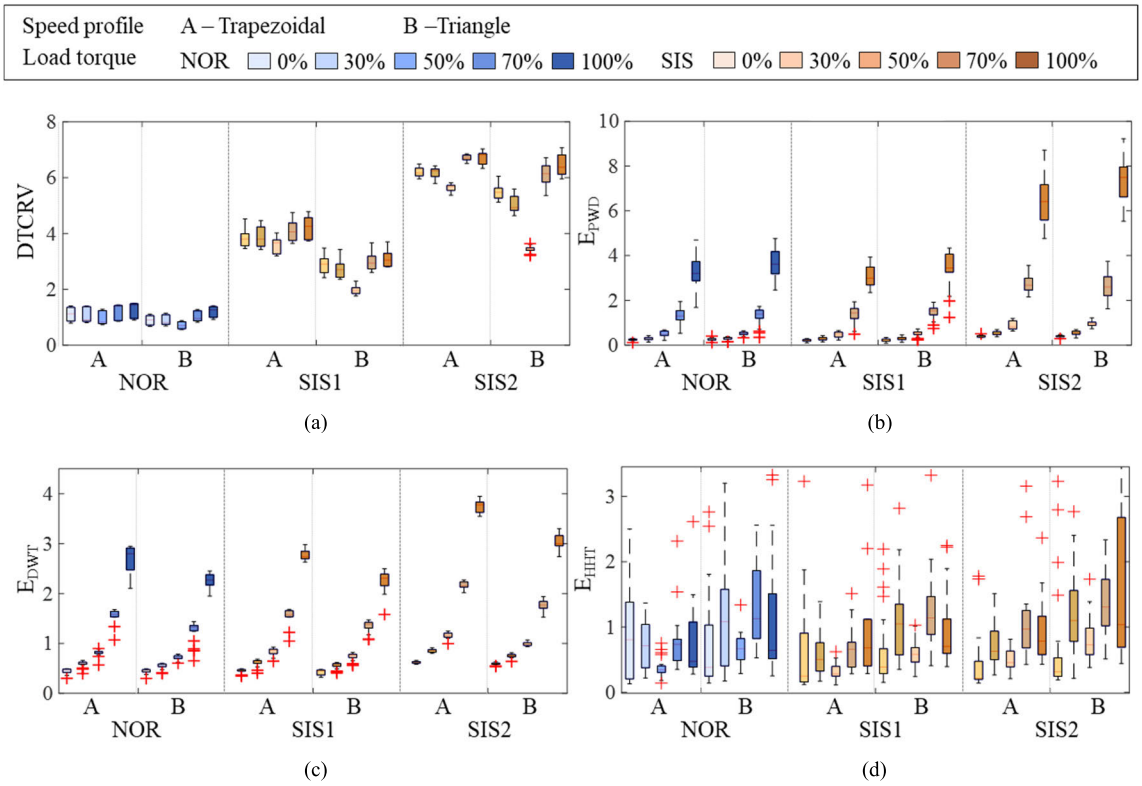

FIGURE 7. Results of the proposed and the conventional methods under SIS: (a) DTCRV, (b) PWD, (c) DWT, (d) HHT.

TABLE 5 quantitatively shows the performance of SIS detection using two measures for class separation: 1) the Fisher discriminant ratio (FDR) [42] and 2) the probability of separation (PoS) [43]. DTCRV had an overwhelmingly better separation capacity in both measures. The outstanding performance of DTCRV was possible because its techniques,

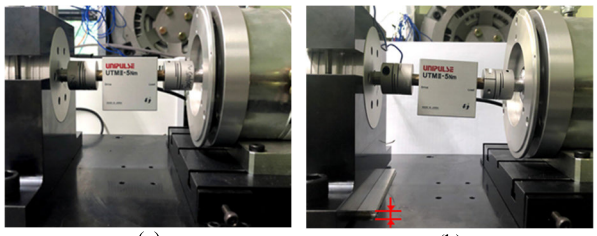

(a) (b)

FIGURE 8. The test rig for misalignment: (a) NOR and (b) MSGN2.

which suppress the drive-related components, enhanced its sensitivity to the fault. Further, it is noticeable that the unit computing time of DTCRV was significantly faster than that of E_{PWD} and E_{HHT}, as can be seen in TABLE 5. All the time-costs were measured under i7-6700K CPU with 32GB RAM. The faster computing time of DTCRV than E_{PWD} was attributed to its calculation in the time-domain only. The repeated convolutions to convert signals in the time-domain to the time-frequency domain are not required for DTCRV. Also the reason for the fast computing time of DTCRV than E_{HHT} was that the procedure of determining the drive-related signal of DTCRV was much simpler than calculating local maxima and local minima. The results of DTCRV in 50% load torque conditions were sometimes low, as shown in Fig. 7(a). These results could be explained based on the influence of the control system in deceleration. The motors were forced to stop in the commanded time in different load torque levels and the load torques were also used in deceleration. When the load torque was low, the output torque had to be replenished for the on-time stop; when the load torque was high, the output torque for hindering fast deceleration was required. This explanation was supported by checking the deceleration regions of Fig. 5 and 6. However, it is important to note that DTCRV showed remarkable performance when subjected to both speed profile and load torque variations, although it was affected by the control in deceleration.

C. EXPERIMENT 2: MISALIGNMENT (MSGN)

To investigate a mechanical fault, MSGN was emulated by rearranging the vertical height of the motor, as shown in Fig. 8. Two fault levels (2 mm and 4 mm) were used in the experiment.

Fig. 9 shows the procedure for calculating DTCR from the raw current signal in several driving conditions of MSGN2. Comparing the raw current signals in Fig. 9 with those of the corresponding operating conditions in NOR (shown in Fig. 5), the amplitude became larger. This was because much output torque was required to compensate for the interference, which MSGN induced to normal output torque. Also, $ENV(t)$s of MSGN showed more peak shapes, while those of SIS had the form of modulation, as shown in the enlarged parts of Fig. 6(b) and Fig. 9(b), respectively. The large fluctuation of $ENV(t)$ sometimes caused the oscillated $G(t)$, as can be seen in Fig. 9 (a, b). Nevertheless, it was not hard to divide sections because the peak points of $G(t)$ were determined relatively. Comparing DTCRs in Fig. 9 with those of Fig. 6, DTCRs in MSGN more fluctuated than those of SIS.

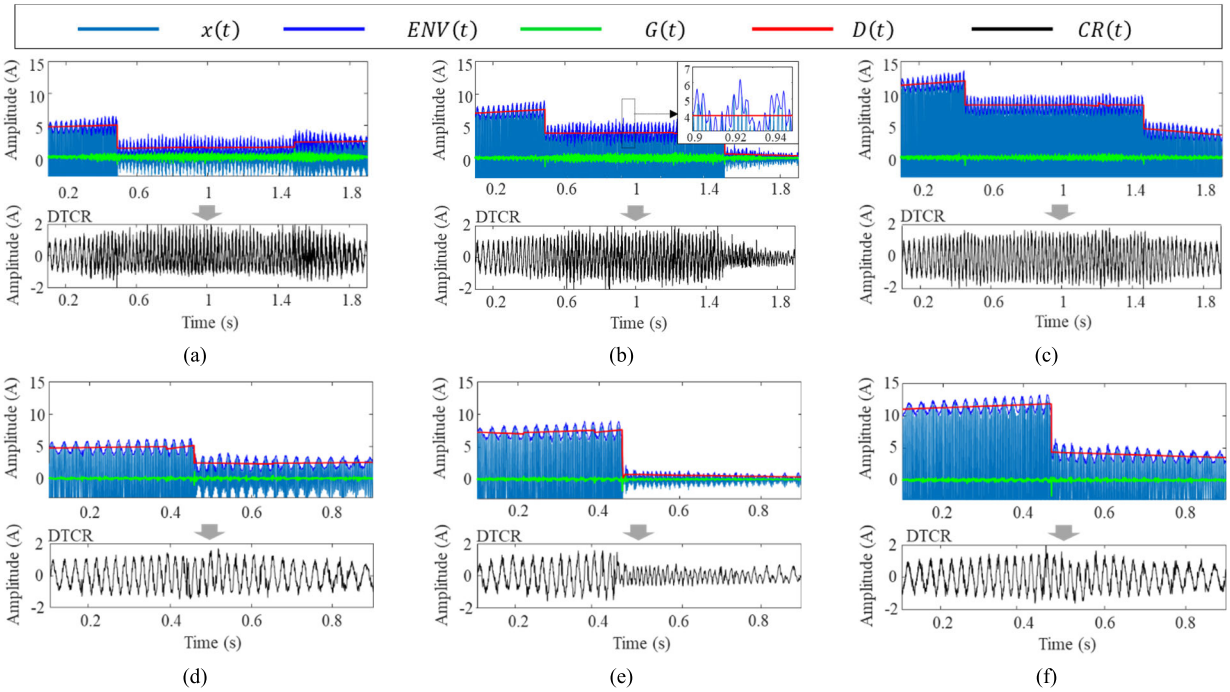

FIGURE 9. The procedure for calculating DTCR in MSGN2: [profile, load torque] (a) [Trapezoidal, 0%], (b) [Trapezoidal, 50%], (c) [Trapezoidal, 100%], (d) [Triangle, 0%], (e) [Triangle, 50%], and (f) [Triangle, 100%].

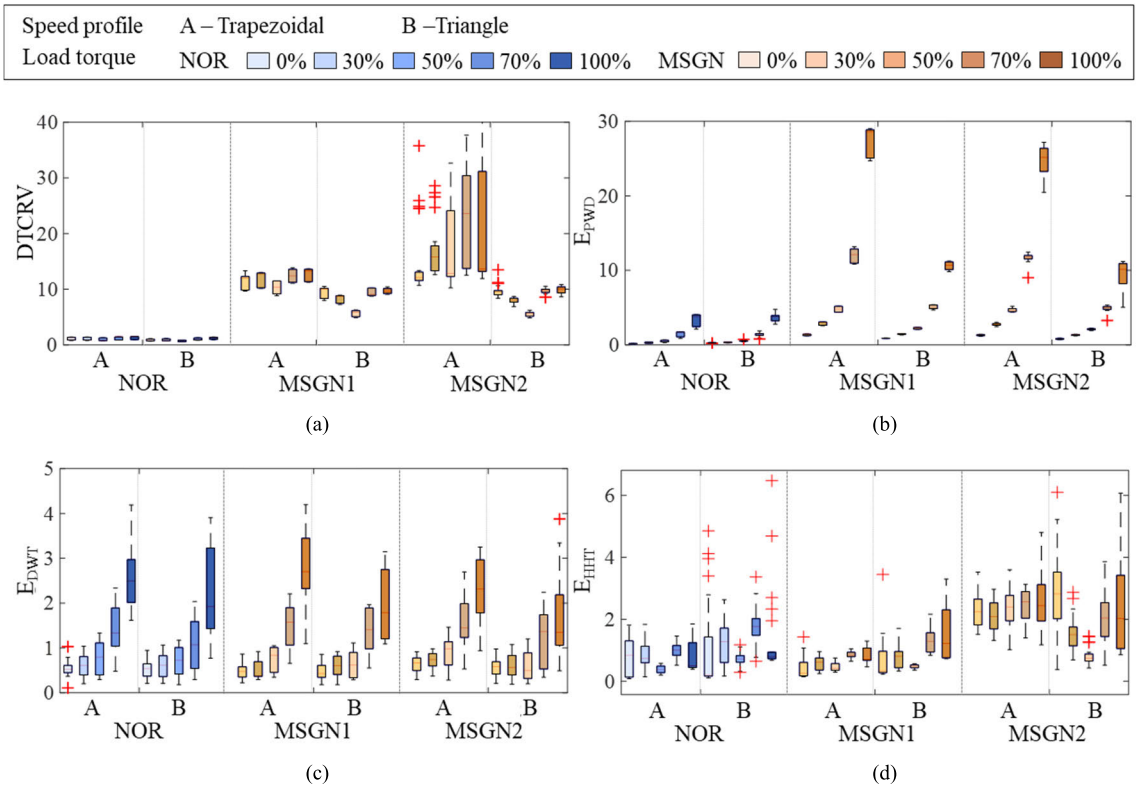

FIGURE 10. Results of the proposed and the conventional methods under MSGN: (a) DTCRV, (b) PWD, (c) DWT, (d) HHT.

Through this large fluctuation, we can suggest that DTCR is more sensitive to mechanical faults.

Fig. 10 shows the results of each feature (i.e. E_{PWD}, E_{DWT}, E_{HHT}, and DTCRV), as determined using the PWD, DWT, HHT, and the proposed DTCRV methods, respectively. The normalization of each feature and the calculation of the conventional features were conducted in the same way described in Section IV-B. For E_{PWD}, the magnitudes of the coefficients of PWD around $f_s \pm f_r/2$ were mean-squared over time. For E_{DWT}, the seventh detail signal *d7* was selected and calculated as the sum of squares because the frequency band of *d7* was from 250 Hz to 500 Hz, which was able to contain the time-varying characteristic frequency $f_s \pm f_r$. For E_{HHT}, the second IMF of the raw current signal was extracted, and the variance of its instantaneous amplitude was computed. Like the results in Section IV-B, the behaviors of DTCRV were robust to variable speed profile and load torque conditions. From the results that E_{PWD} and E_{DWT} were proportional to the load torque level as shown in Fig. 10(b, c), the influence of the load torque levels on E_{PWD} and E_{DWT} seemed to be higher than that of MSGN. E_{PWD} could detect MSGN at 70% and 100% load torque levels; however, MSGNs under 50% or less load torque levels were not distinguishable from NOR at 100% load torque level (See Fig. 10(b)). E_{DWT} had a significant variance in each operating condition due to the insufficient signal decomposition; the characteristics of MSGN were concealed in the load torque conditions (See Fig. 10(c)). As shown in Fig. 10(d), E_{HHT} was able to detect MSGN2 because the drive-related components were separated in the first IMF; however, E_{HHT} could not detect MSGN1. While HHT was not able to detect SIS, it showed decent performance in MSGN detection. Through these irregular result of HHT, the effect of instability that the empirical procedure of HHT causes could be confirmed.

TABLE 6 quantitatively describes the performance and unit computing time of all the features, which were measured in the same state as in Section VI-B. The result of high FDR and PoS values with the small time-cost in DTCRV confirmed its outstanding performance compared to the other three features. Though both MSGNs showed the higher DTCRV values, as compared to those of NOR, the DTCRVs of MSGN1 and MSGN2 did not linearly increase, and DTCRVs of MSGN2 were spread in the trapezoidal speed profile case (see Fig. 10(a)). It seems possible that these results were due to the slight misalignment that resulted from the repeated experimental disturbances. However, it is noticeable that the proposed DTCRV approach can promptly detect the incipient MSGN without any information about the fault or driving conditions.

D. REMARKS OF DTCRV RESULTS

Through the results of two experimental studies, the DTCRV method have shown the noticeable performance as below:

TABLE 6. Performance of MSGN detection and average time-cost for calculating one feature.

	Features	DTCRV (Proposed)	E_{PWD} [19]	E_{DWT} [26]	E_{HHT} [32]
Performance measure	FDR	2.986	0.258	0.001	0.222
	PoS	0.873	0.433	0.016	0.254
Time-cost		0.007±0.002 sec	44.113±3.396 sec	0.004±0.007 sec	0.027±0.007 sec

1) DTCRV was able to detect a fault without being affected by the driving condition (i.e., speed profiles and load torque levels), while the conventional methods were dominated by the driving conditions.
2) Neither motor-specific information nor parameter settings for signal decomposition were required to calculate DTCRV.
3) The computational cost of DTCRV was low.

V. CONCLUSION

This paper proposed a new, drive-tolerant current residual variance (DTCRV) method for detecting faults under operational speed and load torque conditions. The proposed method extracted the envelope of the raw current signal to emphasize its modulation, which contains both drive-related and fault properties. Then, drive-related components were estimated using gradient-based linear regression. The DTCR, which was taken by subtracting drive-related components from the envelope signal, highlighted the unexpected oscillations from the abnormal state. Finally, the variance was computed to quantify the variation of the DTCR. Two case studies that investigated the different fault modes (i.e., SIS and MSGN) were demonstrated to validate the performance of the proposed approach. These case studies showed that the DTCRV method could detect each fault under several driving conditions, while the conventional methods using PWD, DWT, and HHT suffered from the effect of driving conditions. The primary benefits of the proposed method are that it can detect an incipient abnormal state without requiring information about the fault or the driving condition. Moreover, the computational time of DTCRV is far less than that of the TFA-based approach, motor domain knowledge is not required, and the number of parameters that DTCRV demands is also less than that of both TFA-based and signal decomposition-based approaches. Future work can be conducted to identify fault modes considering control constraints under a wider range of driving conditions. Further, DTCRV will be investigated and applied to other motors embedded in industrial robots or electric vehicles.

REFERENCES

[1] G. Ahn, J. Lee, C. H. Park, M. Youn, and B. D. Youn, "Inter-turn short circuit fault detection in permanent magnet synchronous motors based on reference voltage," in *Proc. IEEE 12th Int. Symp. Diag. Electr. Mach., Power Electron. Drives (SDEMPED)*, Aug. 2019, pp. 245–250.
[2] D.-H. Kim, T. J. Y. Kim, X. Wang, M. Kim, Y.-J. Quan, J. W. Oh, S.-H. Min, H. Kim, B. Bhandari, I. Yang, and S.-H. Ahn, "Smart machining process using machine learning: A review and perspective on machining industry," *Int. J. Precis. Eng. Manuf.-Green Technol.*, vol. 5, no. 4, pp. 555–568, Aug. 2018.
[3] Y. Wu, B. Jiang, and Y. Wang, "Incipient winding fault detection and diagnosis for squirrel-cage induction motors equipped on CRH trains," *ISA Trans.*, vol. 99, pp. 488–495, Apr. 2020.
[4] C. H. Park, J. Lee, G. Ahn, M. Youn, and B. D. Youn, "Fault detection of PMSM under non-stationary conditions based on wavelet transformation combined with distance approach," in *Proc. IEEE 12th Int. Symp. Diag.Electr. Mach., Power Electron. Drives (SDEMPED)*, Aug. 2019, pp. 88–93.
[5] I. Shin, J. Lee, J. Y. Lee, K. Jung, D. Kwon, B. D. Youn, H. S. Jang, and J.-H. Choi, "A framework for prognostics and health management applications toward smart manufacturing systems," *Int. J. Precis. Eng. Manuf.-Green Technol.*, vol. 5, no. 4, pp. 535–554, Aug. 2018.
[6] Z. Gao, C. Cecati, and S. X. Ding, "A survey of fault diagnosis and fault-tolerant techniques—Part I: Fault diagnosis with model-based and signal-based approaches," *IEEE Trans. Ind. Electron.*, vol. 62, no. 6, pp. 3757–3767, Jun. 2015.
[7] Y. Wu, B. Jiang, N. Lu, H. Yang, and Y. Zhou, "Multiple incipient sensor faults diagnosis with application to high-speed railway traction devices," *ISA Trans.*, vol. 67, pp. 183–192, Mar. 2017.
[8] G. Liu, Y.-Y. Cao, and X.-H. Chang, "Fault detection observer design for fuzzy systems with local nonlinear models via fuzzy Lyapunov function," *Int. J. Control, Autom. Syst.*, vol. 15, no. 5, pp. 2233–2242, Oct. 2017.
[9] J. Xiong, X. H. Chang, J. H. Park, and Z. M. Li, "Nonfragile fault-tolerant control of suspension systems subject to input quantization and actuator fault," *Int. J. Robust Nonlinear Control*, vol. 30, no. 16, pp. 6720–6743, 2020.
[10] P. Gangsar and R. Tiwari, "Signal based condition monitoring techniques for fault detection and diagnosis of induction motors: A state-of-the-art review," *Mech. Syst. Signal Process.*, vol. 144, Oct. 2020, Art. no. 106908.
[11] B. Saritha and P. A. Janakiraman, "Sinusoidal three-phase current reconstruction and control using a DC-link current sensor and a curve-fitting observer," *IEEE Trans. Ind. Electron.*, vol. 54, no. 5, pp. 2657–2664, Oct. 2007.
[12] C. H. Park, H. Kim, J. Lee, G. Ahn, M. Youn, and B. D. Youn, "A feature inherited hierarchical convolutional neural network (FI-HCNN) for motor fault severity estimation using stator current signals," *Int. J. Precis. Eng. Manuf.-Green Technol.*, pp. 1–14, Oct. 2020, doi: 10.1007/s40684-020-00279-3.
[13] Y. Kim, J. Park, K. Na, H. Yuan, B. D. Youn, and C.-S. Kang, "Phase-based time domain averaging (PTDA) for fault detection of a gearbox in an industrial robot using vibration signals," *Mech. Syst. Signal Process.*, vol. 138, Apr. 2020, Art. no. 106544.
[14] J. Park, M. Hamadache, J. M. Ha, Y. Kim, K. Na, and B. D. Youn, "A positive energy residual (PER) based planetary gear fault detection method under variable speed conditions," *Mech. Syst. Signal Process.*, vol. 117, pp. 347–360, Feb. 2019.
[15] Q. Yang, T. Liu, X. Wu, and Y. Deng, "Gear backlash detection and evaluation based on current characteristic extraction and selection," *IEEE Access*, vol. 8, pp. 107161–107176, 2020.
[16] T. A. Shifat and J. W. Hur, "An effective stator fault diagnosis framework of BLDC motor based on vibration and current signals," *IEEE Access*, vol. 8, pp. 106968–106981, 2020.

[17] W. Qian, S. Li, and J. Wang, "A new transfer learning method and its application on rotating machine fault diagnosis under variant working conditions," *IEEE Access*, vol. 6, pp. 69907–69917, 2018.
[18] V. Fernandez-Cavero, D. Morinigo-Sotelo, O. Duque-Perez, and J. Pons-Llinares, "A comparison of techniques for fault detection in inverter-fed induction motors in transient regime," *IEEE Access*, vol. 5, pp. 8048–8063, 2017.
[19] M. Blodt, D. Bonacci, J. Regnier, M. Chabert, and J. Faucher, "On-line monitoring of mechanical faults in variable-speed induction motor drives using the Wigner distribution," *IEEE Trans. Ind. Electron.*, vol. 55, no. 2, pp. 522–533, Feb. 2008.
[20] M. Blodt, J. Regnier, and J. Faucher, "Distinguishing load torque oscillations and eccentricity faults in induction motors using stator current Wigner distributions," *IEEE Trans. Ind. Appl.*, vol. 45, no. 6, pp. 1991–2000, Nov./Dec. 2009.
[21] M. Blodt, M. Chabert, J. Regnier, and J. Faucher, "Mechanical load fault detection in induction motors by stator current time-frequency analysis," *IEEE Trans. Ind. Appl.*, vol. 42, no. 6, pp. 1454–1463, Nov. 2006.
[22] B. Trajin, M. Chabert, J. Regnier, and J. Faucher, "Hilbert versus concordia transform for three-phase machine stator current time-frequency monitoring," *Mech. Syst. Signal Process.*, vol. 23, no. 8, pp. 2648–2657, Nov. 2009.
[23] A. Sapena-Bano, J. Burriel-Valencia, M. Pineda-Sanchez, R. Puche-Panadero, and M. Riera-Guasp, "The harmonic order tracking analysis method for the fault diagnosis in induction motors under time-varying conditions," *IEEE Trans. Energy Convers.*, vol. 32, no. 1, pp. 244–256, Mar. 2017.
[24] M. Riera-Guasp, J. A. Antonino-Daviu, M. Pineda-Sanchez, R. Puche-Panadero, and J. Perez-Cruz, "A general approach for the transient detection of slip-dependent fault components based on the discrete wavelet transform," *IEEE Trans. Ind. Electron.*, vol. 55, no. 12, pp. 4167–4180, Dec. 2008.
[25] B. M. Ebrahimi, M. Javan Roshtkhari, J. Faiz, and S. V. Khatami, "Advanced eccentricity fault recognition in permanent magnet synchronous motors using stator current signature analysis," *IEEE Trans. Ind. Electron.*, vol. 61, no. 4, pp. 2041–2052, Apr. 2014.
[26] M. M. Rahman and M. N. Uddin, "Online unbalanced rotor fault detection of an IM drive based on both time and frequency domain analyses," *IEEE Trans. Ind. Appl.*, vol. 53, no. 4, pp. 4087–4096, Jul. 2017.
[27] T. Ameid, A. Menacer, H. Talhaoui, and Y. Azzoug, "Discrete wavelet transform and energy eigen value for rotor bars fault detection in variable speed field-oriented control of induction motor drive," *ISA Trans.*, vol. 79, pp. 217–231, Aug. 2018.
[28] M. Heydarzadeh, M. Zafarani, M. Nourani, and B. Akin, "A wavelet-based fault diagnosis approach for permanent magnet synchronous motors," *IEEE Trans. Energy Convers.*, vol. 34, no. 2, pp. 761–772, Jun. 2019.
[29] J. Faiz, V. Ghorbanian, and B. M. Ebrahimi, "EMD-based analysis of industrial induction motors with broken rotor bars for identification of operating point at different supply modes," *IEEE Trans. Ind. Informat.*, vol. 10, no. 2, pp. 957–966, May 2014.
[30] J. A. Rosero, L. Romeral, J. A. Ortega, and E. Rosero, "Short-circuit detection by means of empirical mode decomposition and Wigner–Ville distribution for PMSM running under dynamic condition," *IEEE Trans. Ind. Electron.*, vol. 56, no. 11, pp. 4534–4547, Nov. 2009.
[31] A. Mejia-Barron, M. Valtierra-Rodriguez, D. Granados-Lieberman, J. C. Olivares-Galvan, and R. Escarela-Perez, "The application of EMD-based methods for diagnosis of winding faults in a transformer using transient and steady state currents," *Measurement*, vol. 117, pp. 371–379, Mar. 2018.
[32] E. Elbouchikhi, V. Choqueuse, Y. Amirat, M. E. H. Benbouzid, and S. Turri, "An efficient Hilbert–Huang transform-based bearing faults detection in induction machines," *IEEE Trans. Energy Convers.*, vol. 32, no. 2, pp. 401–413, Jun. 2017.
[33] Z. Li, Q. Li, Z. Wu, J. Yu, and R. Zheng, "A fault diagnosis method for on load tap changer of aerospace power grid based on the current detection," *IEEE Access*, vol. 6, pp. 24148–24156, 2018.
[34] S. K. Sul, *Control of Electric Machine Drive Systems*. Hoboken, NJ, USA: Wiley, 2011.
[35] Y. Yao, Y. Li, and Q. Yin, "A novel method based on self-sensing motor drive system for misalignment detection," *Mech. Syst. Signal Process.*, vol. 116, pp. 217–229, Feb. 2019.
[36] D. G. Dorrell, W. T. Thomson, and S. Roach, "Analysis of airgap flux, current, and vibration signals as a function of the combination of static and dynamic airgap eccentricity in 3-phase induction motors," *IEEE Trans. Ind. Appl.*, vol. 33, no. 1, pp. 24–34, 1997.
[37] Y. Park, H. Choi, J. Shin, J. Park, S. B. Lee, and H. Jo, "Airgap flux based detection and classification of induction motor rotor and load defects during the starting transient," *IEEE Trans. Ind. Electron.*, vol. 67, no. 12, pp. 10075–10084, Dec. 2020.
[38] L. Romeral, J. C. Urresty, J.-R. Riba Ruiz, and A. Garcia Espinosa, "Modeling of surface-mounted permanent magnet synchronous motors with stator winding interturn faults," *IEEE Trans. Ind. Electron.*, vol. 58, no. 5, pp. 1576–1585, May 2011.
[39] S.-T. Lee and J. Hur, "Detection technique for stator inter-turn faults in BLDC motors based on third-harmonic components of line currents," *IEEE Trans. Ind. Appl.*, vol. 53, no. 1, pp. 143–150, Jan. 2017.
[40] W. T. Thomson and M. Fenger, "Current signature analysis to detect induction motor faults," *IEEE Ind. Appl. Mag.*, vol. 7, no. 4, pp. 26–34, Jul./Aug. 2001.
[41] *Condition Monitoring and Diagnostics of Machine Systems–Electrical Signature Analysis of Three-Phase Induction Motors*, document ISO 20958:2013, 2014.
[42] C. M. Bishop, *Pattern Recognition and Machine Learning*. New York, NY, USA: Springer, 2006.
[43] B. C. Jeon, J. H. Jung, B. D. Youn, Y.-W. Kim, and Y.-C. Bae, "Datum unit optimization for robustness of a journal bearing diagnosis system," *Int. J. Precis. Eng. Manuf.*, vol. 16, no. 11, pp. 2411–2425, Oct. 2015.

CHAN HEE PARK received the B.S. degree from Seoul National University, Seoul, Republic of Korea, in 2016, where she is currently pursuing the Ph.D. degree with the Department of Mechanical and Aerospace Engineering.

Her research interest includes prognostics and health management (PHM) for electric products. She was the Winner of the PHM Society Data Challenge Competition in 2017 and received the Korean Society of Mechanical Engineers (KSME)-SEMES Innovation Challenge Award in 2017.

JUNMIN LEE received the B.S. degree in biosystems engineering and mechanical engineering from Seoul National University, Seoul, Republic of Korea, in 2013, and the Ph.D. degree in mechanical engineering from Seoul National University, in 2020. His research interests include prognostics and health management for electric machines, power electronics and drives. He was the Winner of the PHM Society Data Challenge Competition, in 2017.

HYEONGMIN KIM received the B.S. degree in mechanical engineering from Seoul National University, Seoul, Republic of Korea, in 2019, where he is currently pursuing the Ph.D. degree with the Department of Mechanical and Aerospace Engineering. His current research interests include prognostics and health management for electric drive systems, and thermal power plant.

CHAEHYUN SUH received the B.S. degree in mechanical engineering from Seoul National University, Seoul, Republic of Korea, in 2020, where he is currently pursuing the M.S. degree with the Department of Mechanical Engineering.

His current research interest includes prognostics and health management for electromechanical drive systems using deep learning approaches.

MYEONGBAEK YOUN received the B.S. degree from Sungkyunkwan University, Seoul, Republic of Korea, in 2018, and the M.S. degree from the Department of Mechanical Engineering, Seoul National University, Seoul, in 2020. His research interest includes prognostics and health management for electric machines using a signal processing approach. He was the Winner in PHM Society Data Challenge Competition, in 2019.

YONGJIN SHIN received the B.S. degree in mechanical engineering from Seoul National University, Seoul, Republic of Korea, in 2019, and the M.S. degree from the Department of Mechanical Engineering, Seoul National University, in 2021. His current research interest includes deep learning approaches for motor diagnosis using class weight optimization.

SUNG-HOON AHN received the Ph.D. degree from Stanford University, in 1997. He has been affiliated with UC Berkeley, Gyeongsang National University, University of Washington, and Hyundai WIA Corporation. He is currently a Full Professor of Mechanical Engineering with Seoul National University. His research interests include smart factories, green manufacturing, soft robotics, 3D printing, composite materials, micro/nano fabrications, renewable energy, and appropriate technology.

BYENG D. YOUN received the Ph.D. degree in mechanical engineering from the University of Iowa, Iowa City, IA, USA, in 2001. He is a Full Professor of Mechanical Engineering with Seoul National University (SNU), and the founder and CEO of OnePredict, Inc. (onepredict.com). His current research interests include prognostics and health management (PHM), engineering design under uncertainty, and energy harvester design. His dedication and efforts in research have garnered substantive peer recognition, resulting in many notable awards, including the Commendation of Prime Minister in 2019, the Shin Yang Academic Award from Seoul National University in 2017, the IEEE PHM Competition Winner in 2014, and the PHM Society Data Challenge Winners in 2014, 2015, 2017, and 2019.